NUMERICAL STUDY OF THE INFLUENCE OF HEAVY DOPING EFFECTS ON THE CURRENT GAIN OF N-P-N POWER TRANSISTORS

A Thesis Submitted

in Partial Fulfilment of the Requirements
for the Degree of

MASTER OF TECHNOLOGY

BY

A. V. CHATURVEDI

to   the

DEPARTMENT OF ELECTRICAL ENGINEERING
INDIAN INSTITUTE OF TECHNOLOGY, KANPUR
MAY, 1984

БЕ-1984- m-CHA- NUM

C E R T I F I C A T E

This is to certify that the work entitled 'NUMERICAL STUDY OF THE INFLUENCE OF HEAVY DOPING EFFECTS ON THE CURRENT GAIN OF N-P-N POWER TRANSISTORS' has been carried out by Mr. A.V. Chaturvedi under my supervision and this has not been sumitted elsewhere for a degree.

(Dr. M.S. TYAGI)
Professor
Department of Electrical Engineering
Indian Institute of Technology
Kanpur
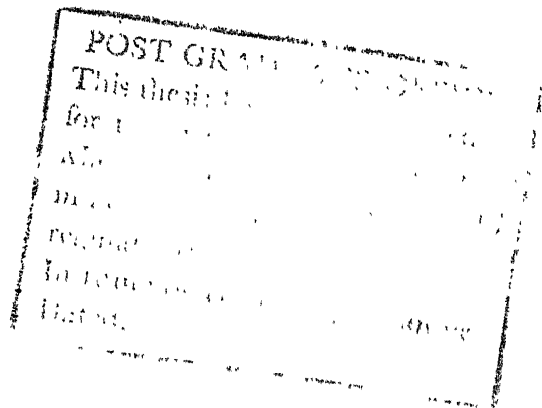
A C K N O W L E D G E M E N T S

Working under the guidance of Dr. M.S. Tyagi has
been a great experience to me and I wish to acknowledge my
deep sense of gratitude to him for his indespensible advices
and critical appraisal.

I express my thanks to Mr. A.K. Gupta for helpful
discussions.

The patient, neat and skillful typing done by
Mr. Yogendra is appreciated.

Finally, I would like to thank all others who have
been, in some way or the other of help in the completion of
this work.

<div align="right">A. V. CHATURVEDI</div>

Table of Contents

LIST OF SYMBOLS

X_{je}, X_{jc} — location of emitter–base/base collector junction from the surface of the transistor.

V_T — Thermal voltage at 300°K.

D_o — Diffusion constant

L_D — Diffusion length

n_{ie} — correction factor to the intrinsic carrier concentration.

Ψ, V — electrostatic potential, applied voltage

q — electronic charge

ε — permittivity

p, n, N — concentration of holes, electrons, ionized impurities.

J_p, J_n, J_T — hole, electron, Total current density

R — recombination rate

G — generation rate

n_i — Intrinsic carrier concentration

k — Boltzman constant

T, T_o — Temperature, 300°K

φ_n, φ_p — electron, hole quasi–Fermi potentials

μ_p, μ_n — hole, electron mobilities

E — Electric field

$R1$ — SRH recombination rate

$R2$ — Auger recombination rate

τ_{po}, τ_{no}	—	equilibrium hole, electron lifetime
δ	—	change in the potential
ψ^{new}	—	corrected value of potential
u	—	general variable
h	—	distance between two successive step points
A	—	coefficient matrix
X	—	unknown vector
Q	—	source term vector
b_m	—	the terms on subdiagonal of A
c_m	—	the terms on diagonal of A
d_m	—	the terms on supradiagonal of A
N_E, N_C, N_B	—	emitter, collector, base surface concentration
α	—	profile parameter
β	—	profile parameter
A_n, A_p	—	Auger Coefficients for electron/hole
α_n, α_p	—	high field generation coefficients for electron/hole
A_E	—	emitter area
W_c	—	length of considered collector region
τ_b, τ_c, τ_e	—	Lifetime of carriers in base/collector/emitter.
N_D^+, N_A^-	—	ionized donor/acceptor atom density.

A B S T R A C T

The heavy doping phenomenons of bandgap narrowing
and Auger recombination have been numerically modeled.
Their individual and relative importance in determining
the current gain of an n-p-n power transistor have been
studied. It is shown that in the devices with emitter
junction depths of 2μm or less bandgap narrowing dominates
all other mechanisms. SRH recombination has the most
effect on current gain in the devices with emitter junction
depths of 4μm or more.

CHAPTER 1

INTRODUCTION

The operation of a junction transistor depends on the introduction and transport of minority carriers across the base region of the transistor. In the design of an efficient transistor, it is necessary to contrive that the emitter current is predominantly a current of minority carriers emitted into the base rather than a current of majority carriers withdrawn from the base. For this requirement to be met the emitter side of the emitter base junction must be more heavily doped than the base side.

In most silicon devices, the emitter doping levels in excess of 10^{18} cm^{-3} are found. At such high doping levels, the basic parameters such as the density of states, the width of the forbidden energy gap, the minority carrier mobility and the minority carrier lifetime strongly differ from their values in a lowly doped crystal. The bandgap of silicon is reduced, the electron and hole mobilities decrease and the minority carrier lifetime becomes lower at heavy doping levels.

These heavy doping effects have to be taken into account in the modeling of transistor. The electron and hole mobilities in silicon as a function of dopant concentration and temperature are important parameters for device

design and analysis. The importance of the minority carrier lifetime is obvious . It influences dc as well as transient performance. The impact of bandgap narrowing effects on device performance is nearly as obvious. The bandgap shrinkage and the deformation of band structure results in an increase in the pn product with increasing impurity concentration. Keeping in mind that most electrical quantities of interest, such as currents and minority carrier storage, are proportional to this product one understands the impact of these effects on the device performance. Heavy emitter doping has a detrimental effect on many transistor parameters. In addition to decreasing the transistor gain and increasing the temperature dependence of gain, it also results in a higher noise figure. The excess noise generally attributed to surface effects is substantially larger for heavily doped emitters.

1.1 Literature Survey :

Mertens et al[1],[2] have considered the heavy doping effects by modifying the device transport equations . They have calculated the transistor current gain after solving numerically these modified transport equations. Slotboom et al [3] have given an emperical formula for bandgap shrin-

kage, which can be used for concentrations in the range of $4 \times 10^{15} - 2.5 \times 10^{19}$ cm^{-3}. Lanyon et al[4] have derived an analytical expression for bandgap narrowing which may be used for modeling of the bandgap shrinkage. The expression is in good agreement with experimental results in the doping range of 3×10^{17} to 1.5×10^{20} cm^{-3}. Possin et al [5] have suggested some modification in the classical device equations for including the bandgap narrowing. They suggest using an effective electric field term in the equations. Gaur et al[6] have modeled the heavy doping effects by including Auger recombination and correction to intrinsic carrier concentration. The results of measurements of bandgap narrowing done by a number of investigators is shown in Fig. 1.

Shibib et al[7] have shown that Auger recombination alone cannot explain the common emitter current gain in bipolar transistors. Other physical mechanisms in addition to Auger recombination have to be considered to account for the observed values of current gain. The Auger coefficients calculated by various authors are tabulated in Table 1. Numerical treatment of Auger recombination has been done by [8 - 10]. Recently Polsky et-al[11] have numerically simulated the bipolar semiconductor devices taking into account heavy doping effects and Fermi statistics.

1.2 Preview :

The objective of the present work is to simulate the heavy doping effects of bandgap narrowing and Auger recombination in order to determine their individual and relative influence on the current gain of a n-p-n power transistor. The basic device equations in one dimension with required modification for inclusion of bandgap narrowing and Auger recombination effects, have been solved for the transistor and its current gain for the given impurity profile has been determined in the presence of different combinations of these effects. Chapter two presents the physical basis for the modeling. Chapter three discusses first the general philosophy of modeling and various approaches to the modeling of bipolar devices. The approach followed for the modeling of n-p-n power transistor is then described. Chapter four presents the results obtained and the discussion of the results. Plots of current gain versus emitter junction depths and current gain versus collector currents are presented. Chapter five summarizes the main results of the work. The computer programmes written in Fortran have been included in the Appendix.

THEORATICAL BACKGROUND

2.1 Energygap :

At heavy doping levels, the number of mobile carriers
is very large and they are quantum mechanically indistinguish-
able i.e. one particle cannot be distinguished from the
other. The energy distribution of carriers in such condi-
tions obey the Fermi-Dirac statistics rather than Maxwell-
Boltzman statistics which is obeyed at lower doping levels
when the particles are distinguishable.

Since there is a large number of carriers in the
crystal, the separation between them is very small and the
interaction between carriers, and carriers and ionized ions
becomes prominent. The majority electrons (for n-type Si)
screen the donor ions through Columb interaction and reduce
the ionization energy of the donor. This results in donor
level moving up toward and ultimately into the conduction
band. Similarly, when majority electrons interact with mino-
rity holes, the hole potential energy is reduced and the
valence band edge moves toward conduction band. The electron-
electron interaction is due to their spin motion and there is
an exchange energy associated with this motion. The effect
of this interaction on energy band is that the conduction band
edge moves downward.

The distribution of impurity atoms in the crystal at
heavy dopings is not uniform. The crystal is disordered and
the distribution of donor ions is random. This random dis-
tribution causes fluctuations in local electrostatic potential
and variations in the energy of the electronic states in both
the conduction and valence band results. These variations
in energy cause a spatially dependent distortion of quantum
density of states. Concommittantly the statistical average
over the entire lattice, of the density of states, which
defines the macroscopic properties of the semiconductor,
showstailing into the energy gap, of both the conduction and
valence band density of states. The bands are not parabolic
near the extrema in such cases and the energy gap is effecti-
vely reduced.

The discrete donor levels at low dopings levels,
spread to form a band at high doping levels. This is because
the spacing between the impurity atoms is small. This allows
the electron wave function at the bound states to overlap.
The random distribution of the donors also results in vari-
ation in the donor energy level and formation of impurity
band tails. The effect of the impurity band formation on
band structure is negligible since the impurity bands are
narrow, there is only a small number of electrons in them,
and the mobility of these electrons is small.

The measurements of bandgap narrowing have yielded
two types of bandgaps. The measurement of optical absorp-
tion give the 'optical' energy gap. The change in this bandgap
is due to many body effects such as the interaction of elec-
trons with electrons. and with holes. The measurements of
minority carrier concentrations yield the 'electrical' energy
gap. The change in this gap is due to both many body effects
and band tailing effects. This change in 'electrical' energy
gap defines the effective intrinsic carrier density n_{ie}.

2.2 Auger Recombination :

The band-to-band Auger recombination is a three carrier
effect. In this process, the recombining e-h pair gives its
energy either to an electron in the conduction band (called
e-e-h process) or to a hole in the valence band (called e-h-h
process). The Auger recombination predicts lifetime inversely
proportional to the square of the majority carrier concen-
tration in degenerate as well as in non-degenerate semicon-
ductors.

CHAPTER 3

DEVICE MODELING

Modeling is the art of characterization of the behaviour of a physical process. The device model attempts to describe the internal and the terminal electrical behaviour of the device. There are two broad categories into which modeling can be devided. Both these approaches are commonly used in device modeling. The parameters of an empirical model are generally obtained through a study of the experimentally measured behaviour of the device as viewed from its terminals. This involves application of curve fitting techniques to obtain functional relationships between the terminal quantities of interest. The physical model, on the other hand, is based on an analysis of the basic internal physical mechanism of the device. It enables an insight into the working of the device and gives an excellent qualitative picture of the effects of changes in material and structural parameters on its terminal, electrical behaviour.

Models have also been developed which make use of a combination of the two approaches mentioned above. The physics of the device is used as a guide to its terminal description. As far as the device engineer is concerned, it is the physically oriented model that is more important.

This is because only this type of model enables the opti-
mization—designing the device so as to improve some specific
aspect of circuit performance to be performed.

3.1 Transistor Modeling :

The following three basic approaches are in use for
modeling a transistor.

(a) The classical analytic approach : The models developed
using this approach are simple, can be analytically manupula-
ted, and are directly related to the physics of the device.
However, they do not accurately represent the behaviour of
the device under all conditions of operation. An example of
this type of approach is the well-known Schockley model of
a transistor.

(b) The total computer approach : This approach is based on
a rigorous solution of the basic semiconductor equations.
The results obtained are highly accurate.

(c) The regional approximation method : This approach is
based on the division of the transistor structure into well-
defined physical regions. Different approximation are made
on the basic semiconductor equations in the different regions
and these equations are then solved either analytically or

on the computer. The self-consistency of the approximation is checked from point to point.

The present modeling follows the total computer approach. The basic semiconductor equations are solved by finite difference method after including modifications due to heavy doping concentrations. The bandgap narrowing is modeled as correction to the intrinsic carrier concentration and the modeling of Auger recombination is done by adding an expression of Auger recombination rate to the expression of SRH recombination. For mobilities expressions are used for its dependence upon carrier concentration and electric field.

3.2 Problem Definition :

The problem is to obtain current gain of an n-p-n power transistor with varying emitter junction depths by solving a set of three basic semiconductor device equations, introduced in the next section. The following information about the device is given; geometry, doping profile, mobilities as function of electric field and impurity density, generation recombination laws including Auger recombination, intrinsic carrier concentration corrected for bandgap narrowing and the appropriate boundary conditions.

3.3 Basic Equations :

The semiconductor transport equations which have to be solved for the steady state behaviour under isothermal conditions are

$$\nabla^2 \Psi \;=\; - \frac{q}{\varepsilon}\,(p-n-N) \tag{1}$$

$$\nabla \cdot J_p \;=\; - q(R - G) \tag{2}$$

$$\nabla \cdot J_n \;=\; + q(R - G) \tag{3}$$

$$J_p \;=\; - q\,\mu_p\,p\,\nabla\Psi - q\,D_p\nabla p \tag{4}$$

$$J_n \;=\; - q\,\mu_n\,n\,\nabla\Psi + q\,D_n\nabla n \tag{5}$$

$$J_T \;=\; J_p + J_n \tag{6}$$

Equation (1) is the Poisson's equation, relating the divergence of the electric flux to the electrostatic charge due to mobile holes (p) and electrons (n) and the ionized impurity atom density ($N = N_D^+ - N_A^-$). The Equations (2) and (3) are the continuity equations for the holes and electrons under steady state conditions. Equations (4) and (5) are the current density relations composed of drift (due to the electric field) and diffusion (due to carrier concentration

gradient) terms. Boltzman approximation of Fermi statistics between the potential and carrier densities have been assumed.

$$n = n_i \exp\left(q\,\frac{(\Psi - \varphi_n)}{kT}\right) \tag{7}$$

$$p = n_i \exp\left(q\,\frac{(\varphi_p - \Psi)}{kT}\right) \tag{8}$$

Quantities φ_p and φ_n in Equations (7) and (8) represent hole and electron quasi-Fermi potentials. The Einstein relation between the carrier mobilities and the diffusion coefficients are assumed to be valid, although this cannot be done for majority carriers in degenerate semiconductors. The dependence of carrier mobilities on electric field and impurity atom density is modeled according to the following formula.[25]

$$\left(\frac{480}{\mu_p}\right)^2 = 1 + \frac{N}{(N/81)+4\times10^{16}} + \frac{(E/6.1\times10^3)^2}{(E/6.1\times10^3)+1.6}$$

$$+ \left(\frac{E}{9.5\times10^4}\right)^2 \tag{9}$$

$$\left(\frac{1400}{\mu_n}\right)^2 = 1 + \frac{N}{\frac{N}{350} + 3 \times 10^{16}} + \frac{\left(\frac{E}{3.5 \times 10^3}\right)^2}{\left(\frac{E}{3.5 \times 10^3}\right) + 8.8}$$

$$+ \left(\frac{E}{7.4 \times 10^3}\right)^2 \tag{10}$$

The Shockley-Read-Hall recombination law is given as follows

$$R1 = \frac{p_n - n_i^2}{\tau_{no}(p+n_i) + \tau_{po}(n+n_i)} \tag{11}$$

The equations for the Auger recombination and high field generation rate are the following

$$R2 = (A_n n + A_p p)(p_n - n_i^2) \tag{12}$$

$$G = n \, \mu_n \, \alpha_n E + p \, \mu_p \, \alpha_p E \tag{13}$$

The values of various constants entering the equations (12) and (13) are given in Table 2.[6]

The transport equations (1) - (6) are normalized into **dimensionless** forms according to normalization factors of Table 3. The normalized set of equation is reduced to three coupled equations in variables Ψ, n and p.

$$\nabla^2 \Psi = n - p - N \tag{14}$$

$$\nabla \cdot (\mu_p(p\nabla\Psi + \nabla_p)) = R - G \tag{15}$$

$$\nabla \cdot (\mu_n(n\nabla\Psi - \nabla_n)) = R - G \tag{16}$$

Equations (7) and (8) in their normalized form reduce to

$$n = \exp(\Psi - \varphi_n) \tag{17}$$

$$p = \exp(\varphi_p - \Psi) \tag{18}$$

Here two variables Φ_p and Φ_n are explicitly introduced

$$\Phi_p = \exp(\varphi_p) \tag{19}$$

$$\Phi_n = \exp(-\varphi_n) \tag{20}$$

These expressions are substituted in the equations (14), (15) and (16) to obtain a new set of equations in the variables Ψ, Φ_p and Φ_n

$$\nabla^2\Psi = \Phi_n \exp(\Psi) - \Phi_p \exp(-\Psi) - N \tag{21}$$

$$\nabla \cdot (\mu_p \exp(-\Psi) \nabla \Phi_p) = R - G \tag{22}$$

$$\nabla \cdot (\mu_n \exp(\Psi) \nabla \Phi_n) = R - G \tag{23}$$

These three coupled equations have been solved by the method outlined next.

3.4 Discretization :

The Poisson's equation (21) is nonlinear in Ψ. This is linearized by assuming

$$\Psi^{new} = \Psi + \delta \tag{24}$$

where Ψ is the potential value of the previous iteration and δ is the correction term. We have

$$\nabla^2\Psi + \nabla^2\delta = \Phi_n \exp(\Psi + \delta) - \Phi_p \exp(-\Psi-\delta) - N$$

$$= \Phi_n \exp(\Psi)[1+\delta+O(\delta^2)] - \Phi_p \exp(-\Psi)[1-\delta+O(\delta^2)] - N$$

$$= \Phi_n \exp(\Psi) - \Phi_p \exp(-\Psi) - N + \delta(\Phi_n \exp(\Psi) + \Phi_p \exp(-\Psi))$$

$$\therefore \quad \nabla^2\delta - \delta(\Phi_n \exp(\Psi) + \Phi_p \exp(-\Psi)) = -\nabla^2\Psi + \Phi_n \exp(\Psi) - \Phi_p \exp(-\Psi) - N \tag{25}$$

Thus neglecting the second and higher order terms equation (25) is considered as a linear differential equation for δ.

The discretization process is achieved with the selection of a uniform step distribution. The finite difference scheme used for reducing the Poisson's equation to the equivalent linear algebraic equation replaces the first derivative at the ith step by the formula

$$\frac{du}{dx}\bigg|_i = \frac{u_{i+1} - u_{i-1}}{2h} \tag{26}$$

and the second derivative by

$$\frac{d^2u}{dx^2}\bigg|_i = \frac{u_{i+1} + u_{i-1} - 2u_i}{2h^2} \tag{27}$$

where u_{i+1}, u_{i-1}, u_i and h are the values of the function is at points $i+1^{th}$, $i-1^{th}$, i^{th} and the distance between two successive points, respectively. Using these formulas, the difference equation at the point 'i' [Fig. 2] is written as

$$[2 + h^2 (\Phi_n(i) \exp(\Psi(i)) + \Phi_p(i) \exp(-\Psi(i)))] \delta_i$$

$$= \delta_{i+1} + \delta_{i-1} + \Psi_{i+1} + \Psi_{i-1} - 2\Psi_i - h^2(\varphi_n(i) \exp(\Psi(i))$$
$$-\varphi_p(i)\exp(-\Psi(i)) - N(i)) \tag{28}$$

The continuity equations are replaced by the difference equation which are obtained by the **box** integration method. The difference equation corresponding to the equation (22) is given as follows

$$(a(i+\tfrac{1}{2})+a(i-\tfrac{1}{2}))\Phi_p(i)=a(i+\tfrac{1}{2})\Phi_p(i+1)+a(i-\tfrac{1}{2})\Phi_p(i-1)$$
$$-h^2(R_i - G_i) \tag{29}$$

where $a = \mu_p \exp(-\Psi)$

The value of 'a' at the point midway between two successive step points is approximated from the known

values of 'a' at these two points. The difference equation
for the relation (23) is similar to (29), but with $a=\mu_n \exp(\Psi)$.

3.5 Solution Procedure :

The difference equations derived in the last section
are applied to every point of the step distribution which
give rise to a system of simultaneous algebraic equation.
These equations can be written in a matrix form as follows

$$AX = Q \qquad\qquad (30)$$

This matrix equation represents a system of linear equations
where each component of the unknown vector 'X' is related
only to adjacent components.

$$b_m \ x_{m-1} + \sigma_m x_m + d_m x_{m+1} = Q_m \qquad\qquad (31)$$

The matrix thus formed is of triple-diagonal form. The matrix
equation is solved directly by a method known as Crout's
method. It is a numerical procedure for forward elimination
followed by backward substitution. The recursion formulas
for the technique are as follows :

$$
\left.
\begin{aligned}
x_n &= p_n \\
x_m &= p_m + h_m \ x_{m-1} \qquad m=n-1, \ n-2 \ \ldots\ldots 1
\end{aligned}
\right\} \qquad (32)
$$

where

$$h_m = \frac{-d_m}{c_m + b_m \, h_{m-1}}; \quad h_1 = -\frac{d_1}{c_1}$$

$$p_m = \frac{Q_m - b_m \, p_{m-1}}{c_m + b_m \, h_{m-1}}; \quad p_1 = \frac{Q_1}{c_1} \right\} \quad (33)$$

The sequence of solution for Ψ, φ_p and φ_n is similar to the one described in reference [12] and is called Gummel's algorithm Fig. (3).

1. An initial guess to Ψ is made from which initial values of φ_p and φ_n are calculated for the given applied voltage.

2. Poisson's equation is solved and new value of Ψ is calculated.

3. Continuity equations are solved to obtain new values of φ_p and φ_n.

4. A test of accuracy is done. If required accuracy is reached the iteration is stopped otherwise go back to step 2.

The current gains are calculated as the ratios of collector current and base terminal current. The effect of

various physical mechanisms with varying emitter size is incorporated by doing the calculation on the above mentioned lines with emitters of different sizes. For this type of computations the total emitter charge is kept constant as the emitter depth is varied.

CHAPTER 4

RESULTS AND DISCUSSION

4.1 Results

The calculations were performed for a power transistor structure which has the following double Gaussian doping profile.

$$N(x) = N_E e^{-\alpha(x/x_{je})^2} + N_C - N_B e^{-\beta(x/x_{je})^2} \qquad (34)$$

where the distance x is measured from the surface of the transistor. The structural and profile parameters of the transistors studied are given in Table [4]. Fig. [4] is a plot of the doping profile.

The material parameters of the transistor are given in Table [5].

The determination of the emitter surface concentration required for equal emitter charge for varying emitter junction depths was done using programe (2).

The results of the calculations performed for the determination of relative importance of various physical phenomenons by varying the emitter depth are tabulated in Table [6] and shown on Fig. (5).

The results of the computations performed for the determination of current gain variation with collector current

in the presence of different physical mechanisms are reported in Table 7 and plotted in Fig. (6).

4.2 Discussion

Fig.(5) shows the dependence of current gain on emitter junction depths in the presence of different combinations of physical processes. The current level in all cases is 8.2A/cm^2. First, the case of 4µm device is considered since it is typical of the overall results. The current gain in the situation when all the mechanisms are contributing, is just below 100. If bandgap narrowing is removed now the current gain increases to 140, showing no significant influence of bandgap narrowing for such a device. If bandgap narrowing is restored and emitter SRH traps are removed, the current gain increase to 425. The removal of Auger recombination in combination of any of the other physical phenomenon, produces only a little further change in the current gain. Thus this shows that SRH recombination is the dominant mechanism influencing the current gain of the devices with emitter junction depth in the range of 4 µm. As the junction depth is further increased, the degree of this effect is also increased.

In the case of the devices with emitter depths of 2µm or less, the direction of these dependencies is same

but the relative magnitudes change. The bandgap narrowing
produces larger changes in the current gain on removal. The
SRH recombination has little effect on current in this range.

The dependence of current gain on emitter junction
depth in the presence of all mechanisms can now be explained.
As the emitter depth is increased from 1 μm to 2 μm the
bandgap narrowing effect weakens and therefore current gain
increases. In the devices of emitter depths greater than
2 μm, current gain decreases with the depth since the effec-
tive emitter charge is lower because the net impurity density
is gradually decreasing in the active emitter region near
the base region.

Figures (6) shows the variation of current gain with
increasing collector current level. Curve (a) shows the same
for the case when all mechanisms are operating; Curve (b),
when Auger recombination has been removed Curve (c), when
bandgap narrowing has been removed and Curve (d), when
bandgap narrowing and Auger recombination both have not been
considered in the analysis. It is clear from the Fig. that
Auger recombination does not have much influence on the
current gain. On removing bandgap narrowing from the analysis,
the resulting current gain increases. Removing Auger recom-
bination alone or alongwith bandgap narrowing produces little
further change in the current gain.

The importance of SRH recombination in determining current gain can be argued as follows. If there is no recombination, bandgap narrowing has virtually no effect on current gain with increasing injection level. Bandgap narrowing enhances the recombination rate if recombination is occuring and this reduces the current gain. As is obvious from the earlier discussion, this is the main effect of bandgap narrowing in devices with emitter junction depths greater than 4 μm. Auger recombination increases with injection level thus reducing the current gain or at best leaving it unchanged. High injection level effects also tend to reduce the current gain. Contrary to all this, SRH recombination decreases with injection level and thus is the only mechanism that can explain the observed initial rise in the current gain with injection level. Bandgap narrowing can affect the recombination rate but alone cannot explain the observations. These arguments are confirmed by the necessity of adjusting the emitter lifetime at different injection level to correctly predict the current gain.

TABLE 1

Auger Coefficients at 300°K from studies in heavily doped silicon

Auger Coefficients $cm^6 sec^{-1}$		Authors and references
A_n	A_p	
1. 1.7×10^{-31}	1.2×10^{-31}	Beck and Conradt [19]
2. 2.8×10^{-31}	9.9×10^{-32}	Dziewior and Schmidt [20]
3. 1.6×10^{-31}	—	Wieder [18]
4. 5×10^{-32}	—	Weaver and Nasby [21]
5. 4×10^{-32}	—	Possin et al [22]
6. 2×10^{-32}	—	Huldt [23]
7. —	1.7×10^{-31}	Leachman [24]

TABLE 2

Values of Coefficients

A_n	1.4×10^{-31} $cm^6 sec^{-1}$
A_p	9.9×10^{-32} $cm^6 sec^{-1}$
α_n	$3.8 \times 10^6 \exp(-1.75 \times 10^6/|E|)$
α_p	$2.25 \times 10^7 \exp(-3.2 \times 10^6/|E|)$

TABLE 3

Normalization Table

Variable	Normalized Quantity	Factor of normalization
Electrostatic Potential	Ψ	$V_t = \dfrac{kT_o}{q} = .026$ V
Quasi-Fermi Levels	φ_n, φ_p	V_t
Voltage	V	V_t
position coordinates	x	$L_D = \sqrt{\dfrac{\varepsilon V_t}{q n_i}} = 34 \mu m$
Charge Concentrations	$n_i, p, n, N, N_B, N_E, N_C$	$n_i = 1.5 \times 10^{10}$ cm^{-3}
Carrier Diffusion Coefficients	$\mu_n V_t, \mu_p V_t$	$D_o = 1$ cm^2/sec
Carrier mobilities	μ_n, μ_p	$\dfrac{D_o}{V_t} = 39.06$ cm^2/sec V
Current densities	J_T, J_p, J_n	$\dfrac{q D_o n_i}{L_D} = 7.05 \times 10^{-7}$ A/cm^2
Generation recombination rate	$R, R1, R2, G$	$\dfrac{D_o n_i}{L_D^2} = 1.3 \times 10^{15}$ /cm^{3}sec
Carrier lifetimes	$\tau_{no}, \tau_{po}, \tau_b, \tau_c, \tau_e$	$\dfrac{L_D}{D_o} = 34 \times 10^{-4}$ sec.

TABLE 4

Structural and profile parameters of the transistor

A_B	x_{jc}	x_{je}	N_E	N_B	N_C	W_C	α	β
$.12$ cm^2	$4.75 \times 10^{-4} cm$	$12.25 \times 10^{-4} cm$	$7 \times 10^{19}/ cm^3$	$2 \times 10^{17}/ cm^3$	$2 \times 10^{14}/ cm^3$	$77.75 \times 10^{-4} cm$	7.061	1.2

TABLE 5

Material parameters of the transistor

τ_b	0.5×10^{-6} sec
τ_c	0.5×10^{-6} sec
$\tau_{e(low\ level)}$	20×10^{-9} sec
$\tau_{e(high\ level)}$	200×10^{-9} sec.

TABLE 6

Current gain for various emitter jn depths.

emitter Jn Depth	All the mechanism contributing	Auger removed	BGN removed	BGN + AR removed	emitter SRH traps removed
	1	2	3	4	5
1µm	104.85	105.97	419.13	421.03	133.21
2µm	118.34	119.23	253.35	255.60	256.73
4µm	98.23	99.55	140.74	142.12	425.19
8µm	55.76	57.31	64.61	65.78	501.25

TABLE 7

Current Gain for different collector currents

Collector current (Amt)	1 All present	2 AR removed	3 BGN removed	4 BGN+AR removed
0.3	63.32	64.87	86.23	87.43
0.5	65.04	65.91	88.45	89.85
0.94	70.25	71.30	94.02	95.28
1.60	72.14	73.48	95.26	96.79
1.8	74.39	75.21	97.83	99.12
2.0	75.46	75.89	98.47	99.89
2.4	75.58	76.02	99.14	100.36
3.0	76.14	77.24	100.42	102.01
4.2	76.53	77.63	101.63	103.42
4.8	77.06	78.12	102.45	104.79
5.3	64.30	65.24	88.01	89.81
5.9	53.21	55.61	77.38	79.52
6.3	45.18	46.72	68.12	70.63
7.5	27.41	29.50	51.48	54.21
9.0	17.59	19.32	41.62	43.72

Fig. 1 Bandgap narrowing measurements

□ Balkanski et al (optical) (13)
x Schmid (optical) (14)
+ Slotboom & de Graft (3)
○ Neugroschel et al (15)
● Wulms (16)
● Tang (17)
* Mertens et al (1)
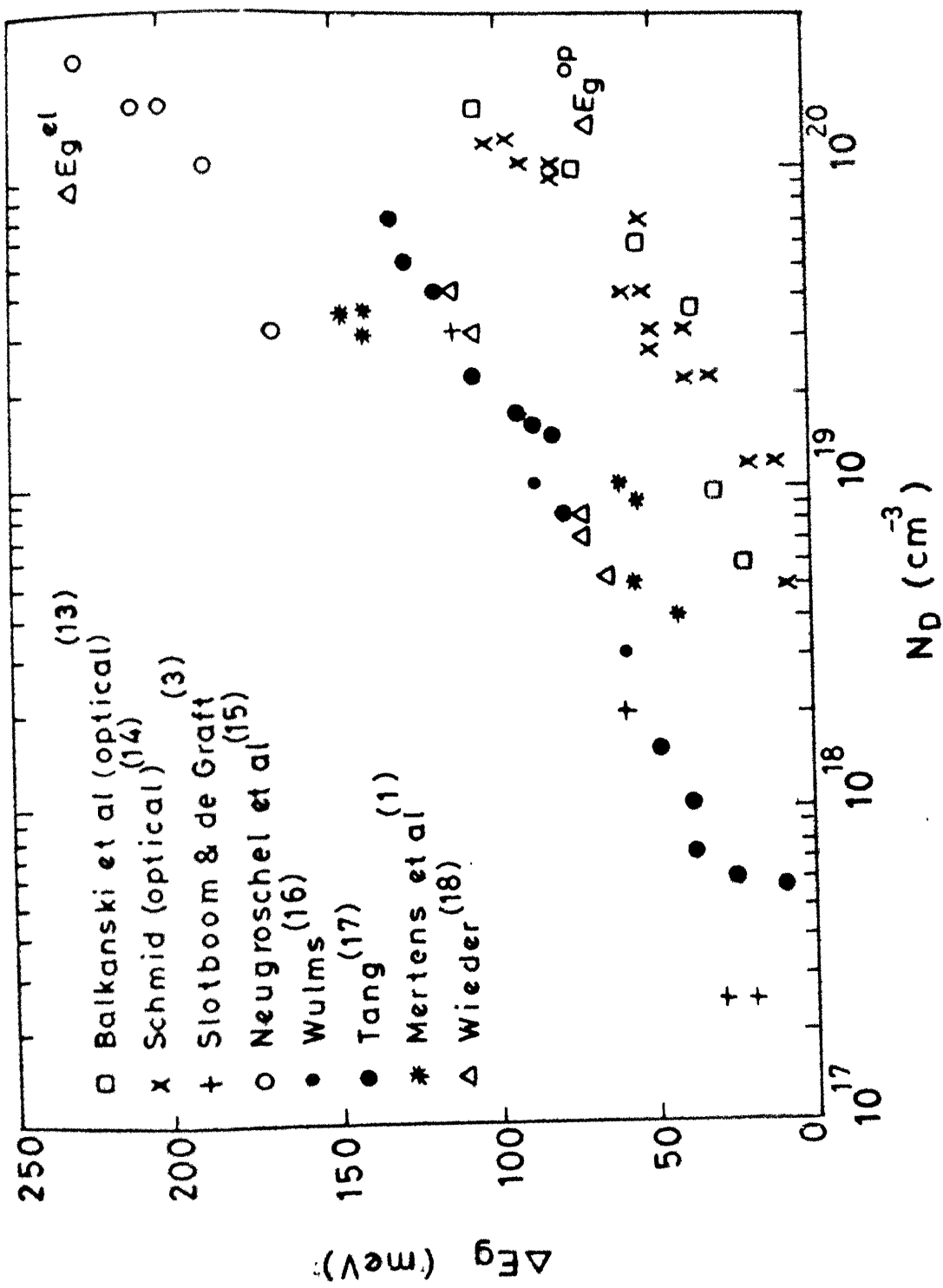△ Wieder (18)

ΔEg^{el}

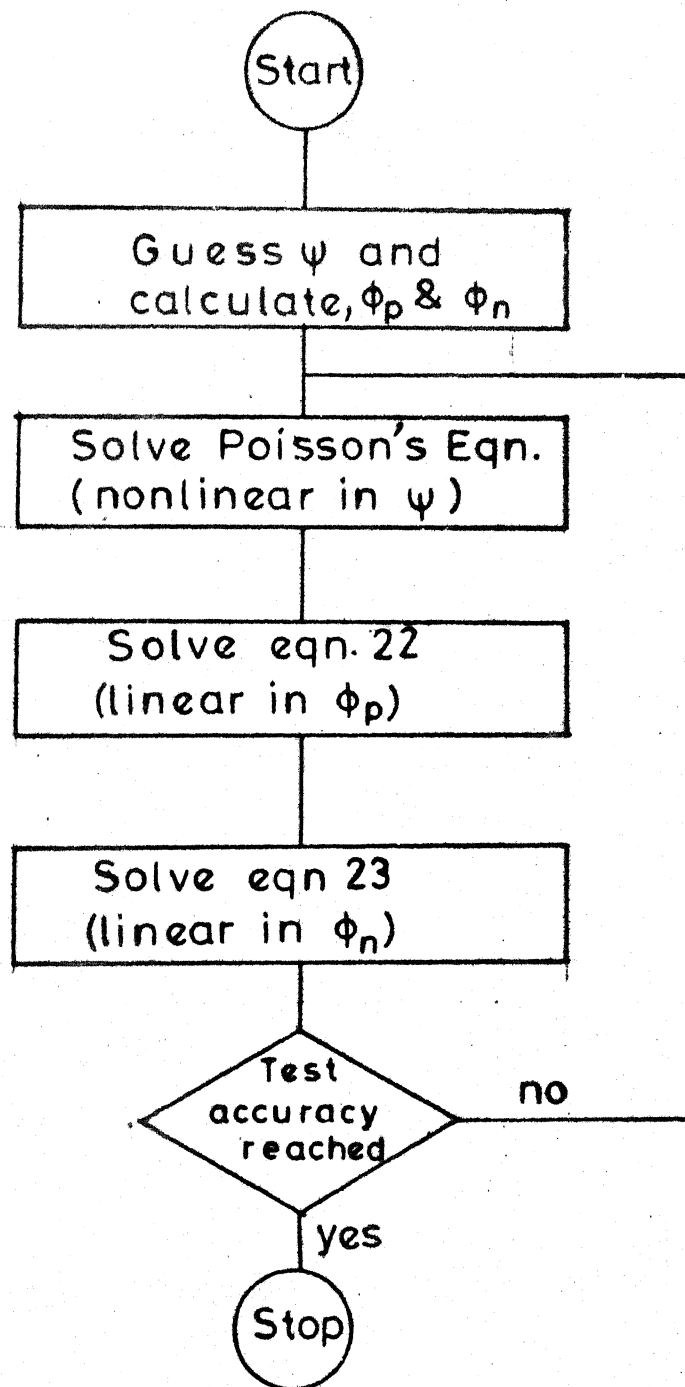ΔEg^{op}

ΔEg (meV)

N_D (cm^{-3})

Fig.3 Flow diagram of the solution
procedure

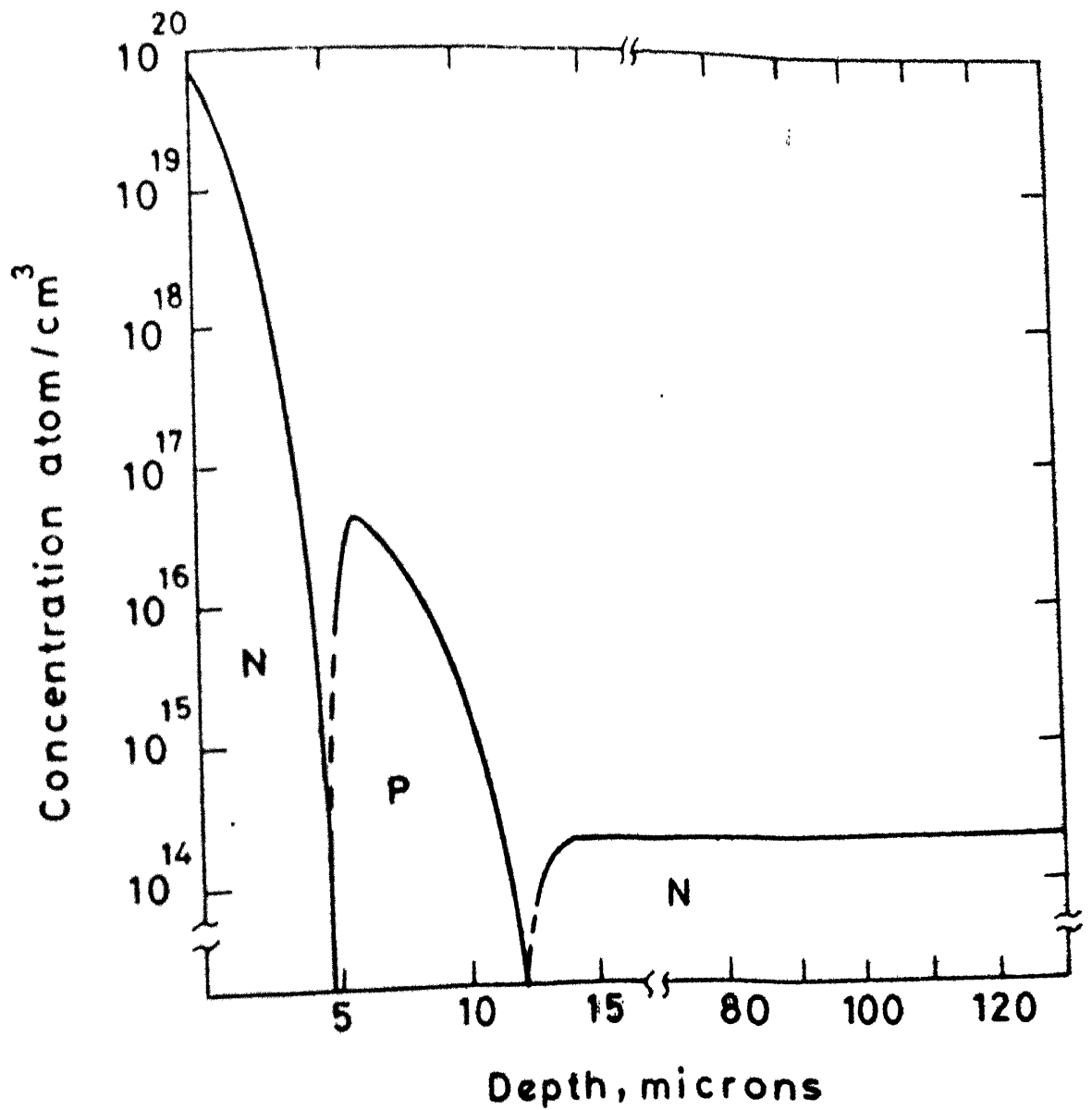Fig.2 Step distribution for discretizing the
device equations

Fig.4 Doping profile for power transister
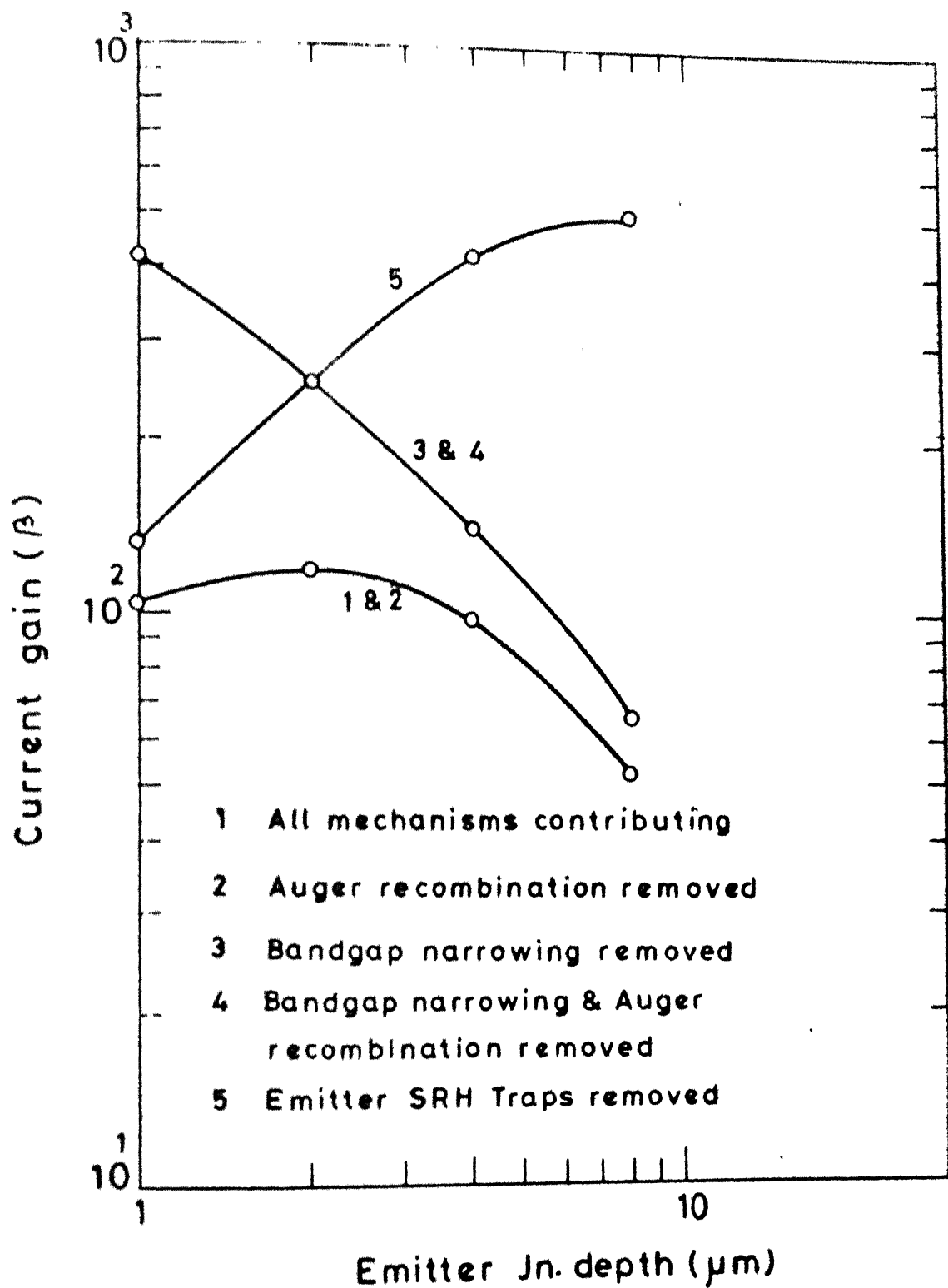
Fig. 5 Calculated current gains for different emitter Jn. depths
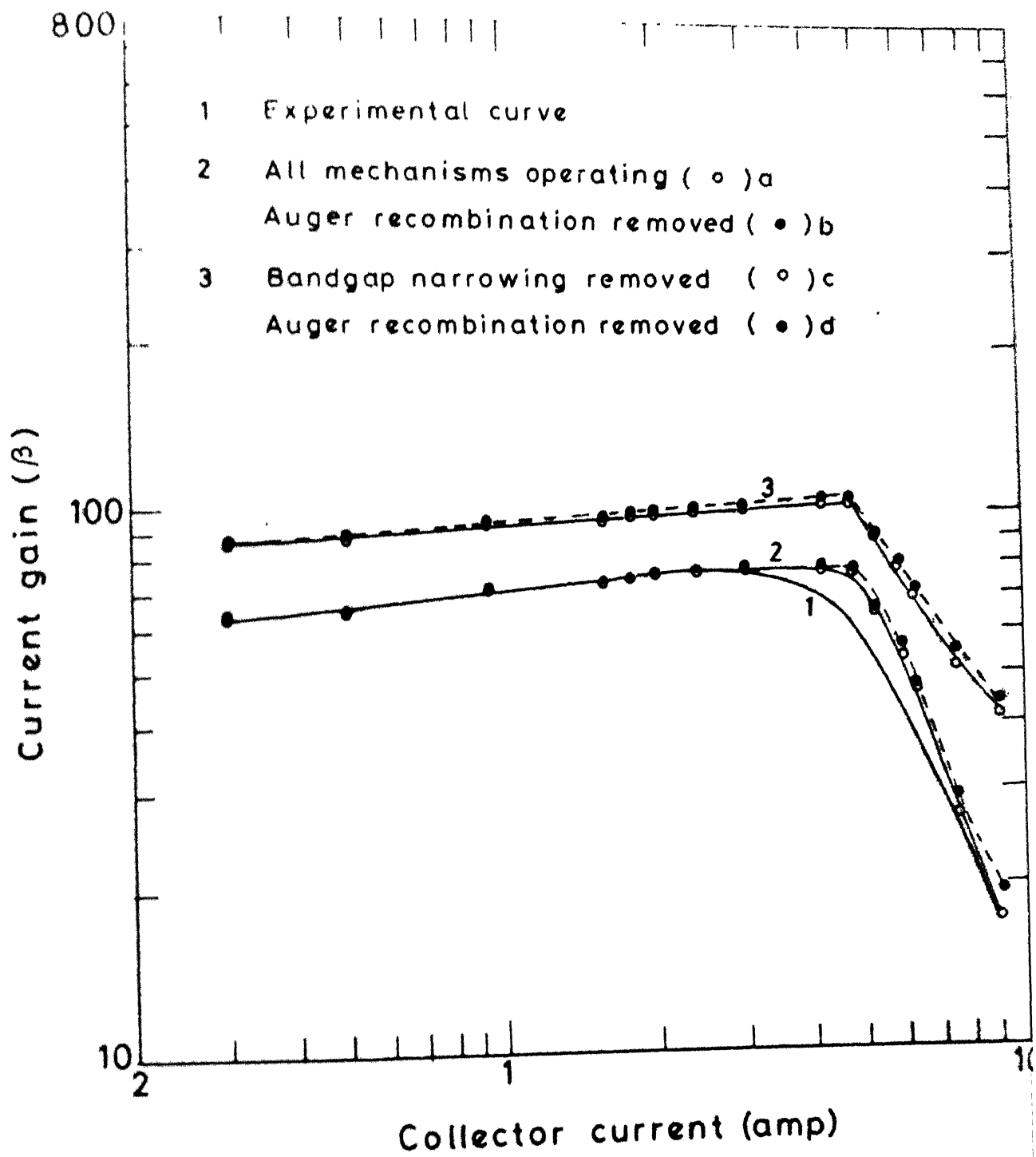
Fig. 6 Calculated current gain for different collector currents

CHAPTER 5

CONCLUSION

It is shown that the bandgap narrowing and SRH recombination effects are the dominant mechanisms in influencing the current gain in transistors. Bandgap narrowing effects dominate all others in the devices with shallow emitters of junction depths of 2 μm or less. The SRH recombination has the most influence on the current gain of the devices with emitters of 4 μm or greater. Auger recombination does not appear to be an important mechanism at the low and moderate injection levels. This is dominated by either bandgap narrowing or SRH recombination and cannot explain the observed current gain in the absence of the above two mechanisms. These conclusions have been arrived at by choosing specific values for the parameters governing the physical mechanisms, for example, bandgap narrowing. The specific choice, however will only effect the results for very small emitter depths since recombination prevents the minority carrier from reaching the portion of the emitter doped at this level for the deeper emitter ($\geq$ 4μm).

R E F E R E N C E S

1. R.P. Mertens, H.J. DeMan, and R.J. Van Overstraeten, 'Calculation of the emitter efficiency of bipolar transitor'. IEEE Trans. Electron Devices, Vol.ED-20, pp 772-778. Sep. 1973.

2. R.J. Van Overstraeten, H.J. DeMan, R.P. Mertens, 'Transport equations in heavily doped silicon}, IEEE Trans. Electron Devices, Vol. ED-20, pp 290-298, Mar. 1973.

3. J.W. Slotboom, and H.C. deGraaff, 'Measurement of bandgap narrowing in silicon bipolar transistors', Solid-State Electron. Vol.19, pp 857-862, 1976.

4. H.P.D. Lanyon and R.A. Tuft, 'Bandgap narrowing in moderate to heavily doped silicon', IEEE Trans. Electron Devices, Vol. ED-26, pp 1014-1018, July 1979.

5. G.E. Possin, H.S. Adler and B.J. Baliga, 'Measurements of bandgap narrowing in heavily doped epitaxial emitters and the modeling of heavily doped silicon', IEEE Trans. Electron. Devices, Vol.ED-27, pp 270-275, 1980.

6. S.P. Gaur, G.R. Srinivasan and I. Anlipou, 'Verification of heavy doping parameters in semiconductor device modeling', IEEE Trans. Electron Devices, Vol. ED-27, pp 276-279, 1980.

7. M.A. Shibib, F.A. Lindholm, and J.G. Fossum, 'Auger recombination in heavily doped shallow-emitter silicon pn-junction solar cells, diodes and transistors, IEEE Trans. Electron Devices, Vol. ED-26, pp 1104-1106, 1979.

8. P.M. Dunbar and J.R. Hauser, 'Theoratical effects of surface diffused region lifetime models an silicon solar cells', Solid-State Electron., Vol.20, pp 697-701, 1977.

9. E.J. McGrath and D.H. Navon, 'Factors limiting current gain in power transistors', IEEE Trans. Electron Devices, Vol. ED-24, pp 1255-1259, 1977.

10. P. Lauwers, J. Van Meerbergen, P. Bulteel, R. Mertens, and R. Van Overstraeten, 'Influence of bandgap narrowing on the perfomance of silicon n-p solar cells', Solid-State Electron, Vol.21, pp 747-752. 1978

11. B.S. Polsky and J.S. Rimshans, '2-D numerical simulation of bipolar semiconductor devices taking into account heavy doping effects and Fermi statistics', SSE, Vol.26, p 275-279, 1983.

12. H.K. Gummel, 'A self-consistent iterative scheme for 1D steady state transistor calculations', IEEE Trans. Electron Devices, Vol. ED-11, pp 455-465, 1964.

13. M. Balkanski, A. Aziza, and E. Amzallog, 'Infrared absorption in heavily doped n-type Si', Phys. Stat. Sol., Vol.31, pp 323-330, 1969.

14. P.E. Schmid, 'Optical absorption in heavily doped silicon', Phys. Rev. B, Vol.23, pp 5531-5536, 1981.

15. A. Neugroschel, S.C. Rao, and F.A. Lindholm, 'A method for determining energy gap narrowing in highly doped semiconductors', IEEE Trans. Electron Devices, Vol. ED-29, pp 894-902, May 1982.

16. H.E.J. Wulms, 'Base current of I^2L transistors, 'IEEE J. Solid State circuits, Vol. SC-12, pp 143-150, 1977.

17. D.D. Tang, 'Heavy doping effects in p-n-p bipolar transistors', IEEE Trans. Electron Devices, Vol. ED-27. pp 563-570, Mar. 1980.

18. A.W. Wieder, 'Emitter effects in shallow bipolar devices: measurement and consequences', IEEE Trans. Electron Devices, Vol. ED-27, pp 1492-1497, Aug. 1980.

19. J.D. Beck and R. Conradt, Solid State Commun. 13, 93 (1973)

20. J. Dziewior and W. Schmidt, Appl. Phys. Lett. 31, 346 (1977)

21. H.T. Weaver and R.D. Nasby, Sandia National Laboratory Reports (1980).

22. G.E. Possin, M.S. Adler and B.J. Baliga, IEEE Trans. ED-27, 983 (1980)

23. L. Huldt, N.G. Nilsson and K.G. Svantesson, Appl. Phys. Lett. 35, 776 (1979).

24. P.W. Loachman, Physica Status Solidi(a) 45, 423 (1978).

25. D.L Scharfetter, and H.K Gummel, " Large - signal analysis of a silicon Read diode oscillator " IEEE Trans. Electron Devices, vol ED-16, pp 64-77, Jan. 1969.

Appendix

Programme No.1 - Solves the device equations

Programme No.2 - Calculates the emitter surface
concentration for different
junction depths.

```
PROGRAM NO.1
 THIS PROGRAM DETERMINES THE COMMON EMITTER CURRENT GAIN FOR AN
 NPN POWER TRANSISTOR AFTER SOLVING THE BASIC SEMICONDUCTOR
 TRANSPORT EQATIONS USING FINITE DIFFERENCE METHOD,GUMMEL'S
 ALGORITHM AND CROUT'S FACTORISATION METHOD.
 VARIABLE DECLARATION
 REAL VT,LD,NI,DO,MU,JO,TO,AA,VA,NE,NB,NC,ALPHA,BETA,H1,H2,XE,XB,
1XC,DOP(900),ENI(900),SI(900),PHIP(900),PHIN(900),PHP(900),PHN(9
200),E(900),P(900),B(900),C(900),D(900),Q(900),DEL(900),DELMX,DE
3LMN,EF(900),R1(900),R2(900),MUP(900),MUN(900),G(900),JN(900),JP
4(900),HFE,EPS1,X(900)
 INTEGER I,J,IT1,Z
 OUTPUT FILE
 OPEN(UNIT=30,DEVICE='DSK',FILE='PP.1')
 NORMALISATION FACTORS
 VT=0.026
 LD=34.E-4
 NI=1.5E10
 DO=1.
 MU=38.65
 JO=7.E-7
 TO=34.E-4
 AA=LD**5
 APPLIED BIAS
 VA=0.0
 ITERATION STOPPING CRITERIA
 IT1M=200
 EPS1=0.1E-04
 CONSIDERATION OF DIFFERENT MECHANISMS
 Z=1 FOR NOMINAL CASE
 Z=2 FOR AR REMOVED
 Z=3 FOR BGN REMOVED
 Z=4 FOR BGN+AR REMOVED
 Z=5 FOR EMITTER SRH REMOVED
 Z=1
 DOPING PROFILE PARAMETERS
 NE=(7.E+19)/NI
 NB=(2.E+17)/NI
 NC=(2.E14)/NI
 BETA=1.2
 ALPHA=ALOG(NE/(NB*EXP(-BETA)-NC))
 XE=(4.75E-4)/LD
 XB=(12.25E-4)/LD
 XC=(90.E-4)/LD
 STEP DISTRIBUTION
```

```
      H1=(0.1E-4)/LD
      H2=H1*H1
      N=XC/H1+1
      DO 10 I=1,N
      X(I)=I*H1
 10   CONTINUE
C     INITIALISATION OF VARIABLES
      DO 20 I=1,N
      DEL(I)=0.0
      PHIP(I)=1.0
      PHIN(I)=1.0
 20   CONTINUE
      CALL DOPING(N,NE,NB,NC,ALPHA,BETA,XE,X,DOP)
      CALL NIEFF(N,VT,Z,NI,DOP,ENI)
      CALL SIINT(N,ENI,DOP,SI)
      IT1=1
 405  CALL COEFF1(N,H2,VA,PHIP,PHIN,SI,DOP,B,C,D,Q)
      CALL CROUT(N,B,C,D,Q,DEL)
      CALL DLM(N,SI,DEL,DELMX,DELMN)
      IF(DELMX.LT.0.1E-04)GO TO 420
      IF(IT1.EQ.IT1M) GO TO 430
      DO 410 J=1,N
      SI(J)=SI(J)+DEL(J)
 410  CONTINUE
      IT1=IT1+1
      GO TO 405
 420  WRITE(30,9000)IT1;GO TO 440
 430  WRITE(30,910)IT1M
 440  DO 450 I=1,N
      SI(I)=SI(I)+DEL(I)
 450  CONTINUE
 500  CALL PHI(N,PHIP,PHIN,NI,SI,P,E,PHP,PHN)
      CALL ELFD(N,H1,VA,SI,EF)
      CALL RSRH(N,H1,XE,Z,P,E,NI,R1)
      CALL RAGR(N,P,E,NI,R2)
      CALL MOBLTY(N,MU,DOP,EF,MUP,MUN)
      CALL HFG(N,P,E,MUP,MUN,EF,G)
      CALL COEFF2(N,H2,VA,Z,MUP,SI,R1,R2,G,B,C,D,Q)
      CALL CROUT(N,B,C,D,Q,PHIP)
      CALL COEFF3(N,H2,VA,Z,MUN,SI,R1,R2,G,B,C,D,Q)
      CALL CROUT(N,B,C,D,Q,PHIN)
      CALL PHI(N,PHIP,PHIN,NI,SI,P,E,PHP,PHN)
      CALL CRNTS(N,H1,VA,MUP,MUN,PHP,PHN,P,E,JN,JP)
      CALL GAIN(N,JP,JN,R1,R2,X,HFE);WRITE(30,*)HFE
 200  STOP
 9000 FORMAT(10X,'POTENTIAL VALUES CONVERGED AFTER',I3,'ITERATIONS')
 910  FORMAT(10X,'NO REQUIRED CONVERGENCE AFTER',I3,'ITERATION')
      END
C     THIS SUBROUTINE DETERMINES DOPING PROFILE
```

```
      SUBROUTINE DOPING(N,NE,NB,NC,ALPHA,BETA,XE,X,DOP)
      DIMENSION DOP(N),X(N),E1(900),E2(900)
      REAL NE,NB,NC
      DO 10 I=1,N
      E1(I)=ALPHA*((X(I)/XE)**2)
      IF(E1(I).GE.20) GO TO 20
      E2(I)=BETA*((X(I)/XE)**2)
      DOP(I)=NE*EXP(-E1(I))+NC-NB*EXP(-E2(I))
      GO TO 10
   20 E2(I)=BETA*((X(I)/XE)**2)
      IF(E2(I).GE.20)GO TO 30
      DOP(I)=-NB*EXP(-E2(I))+NC
      GO TO 10
   30 DOP(I)=NC
   10 CONTINUE
      RETURN
      END
C     THIS SUBROUTINE DETERMINES BGN CORRECTION FACTOR IN NI
      SUBROUTINE NIEFF(N,VT,Z,NI,DOP,ENI)
      DIMENSION DOP(N),ENI(N),F(900),ADOP(900)
      REAL NI
      DO 10 I=1,N
      IF(Z.EQ.3)GO TO 30
      IF(Z.EQ.4)GO TO 30
      XL=(1.E17)/NI
      ADOP(I)=ABS(DOP(I))
      IF(ADOP(I).GE.XL) GO TO 20
   30 ENI(I)=1.
      GO TO 10
   20 F(I)=ALOG(ADOP(I)/XL)
      ENI(I)=EXP((9.E-3)*(F(I)+SQRT(F(I)*F(I)+0.5))/VT)
   10 CONTINUE
      RETURN
      END
C     THIS SUBROUTINE DETERMINES INITIAL VALUE OF ELECTROSTATIC
C     POTENTIAL (SI)
      SUBROUTINE SIINT(N,ENI,DOP,SI)
      DIMENSION ENI(N),DOP(N),SI(N)
      DO 10 I=1,N
      IF(DOP(I).GT.0.0)GO TO 20
      SI(I)=-ALOG(-DOP(I))
      GO TO 10
   20 SI(I)=ALOG(DOP(I))
   10 CONTINUE
      RETURN
      END
C     THIS SUBROUTINE DETERMINES COEFFICIENT MATRIX FOR VARIABLE DEL
      SUBROUTINE COEFF1(N,H2,VA,PHIP,PHIN,SI,DOP,B,C,D,Q)
      DIMENSION PHIP(N),PHIN(N),SI(N),DOP(N),B(N),C(N),D(N),Q(N)
```

```
      DO 10 I=1,N
      IF(I.EQ.1)GO TO 20
      IF(I.EQ.N)GO TO 30
40    B(I)=-1.0
      D(I)=-1.0
      C(I)=2.0+H2*(PHIP(I)*EXP(-SI(I))+PHIN(I)*EXP(SI(I)))
      Q(I)=-H2*(PHIN(I)*EXP(SI(I))-PHIP(I)*EXP(-SI(I))-DDP(I))+SI(I+1)
     1+SI(I-1)-2.0*SI(I)
      GO TO 10
20    SI(I-1)=22.263711
      GO TO 40
30    SI(I+1)=9.4980224+VA
      GO TO 40
10    CONTINUE
      RETURN
      END
C     THIS SUBROUTINE DETERMINES VALUES OF QUASI-FERMI LEVELS AND
C     CARRIER CONCENTRATIONS
      SUBROUTINE PHI(N,PHIP,PHIN,NI,SI,P,E,PHP,PHN)
      DIMENSION PHIP(N),PHIN(N),SI(N),P(N),E(N),PHP(N),PHN(N)
      REAL NI
      DO 10 I=1,N
      PHP(I)=ALOG(PHIP(I))
      PHN(I)=-ALOG(PHIN(I))
      P(I)=NI*EXP(PHP(I)-SI(I))
      E(I)=NI*EXP(SI(I)-PHN(I))
10    CONTINUE
      RETURN
      END
C     THIS SUBROUTINE DETERMINES ELECTRIC FIELD
      SUBROUTINE ELFD(N,H1,VA,SI,EF)
      DIMENSION SI(N),EF(N)
      DO 10 I=1,N
      IF(I.EQ.1) GO TO 20
      IF(I.EQ.N) GO TO 30
40    EF(I)=-(SI(I+1)-SI(I-1))/(2.*H1)
      GO TO 10
20    SI(I-1)=22.263711
      GO TO 40
30    SI(I+1)=9.4980224+VA
      GO TO 40
10    CONTINUE
      RETURN
      END
C     THIS SUBROUTINE DETERMINES SRH RECOMBINATION RATE
      SUBROUTINE RSRH(N,H1,XE,Z,P,E,NI,R1)
      DIMENSION P(N),E(N),R1(N)
      INTEGER J1,Z
      REAL NI
```

```fortran
      J1=XE/H1
      DO 10 I=1,J1
      IF(Z.EQ.5)GO TO 50
      TNO=5.8E-6
      TPO=5.8E-6
      GO TO 60
50    TNO=1.5E-4
      TPO=1.5E-4
60    R1(I)=(P(I)*E(I)-NI*NI)/(TNO*(P(I)+NI)+TPO*(E(I)+NI))
10    CONTINUE
      J11=J1+1
      DO 20 I=J11,N
      TNO=1.5E-4
      TPO=1.5E-4
      R1(I)=(P(I)*E(I)-NI*NI)/(TNO*(P(I)+NI)+TPO*(E(I)+NI))
20    CONTINUE
      RETURN
      END
C     THIS SUBROUTINE DETERMINES AUGER RECOMBINATION RATE
      SUBROUTINE RAGR(N,P,E,NI,R2)
      DIMENSION P(N),E(N),R2(N)
      REAL NI
      AN=3.1E-19
      AP=2.2E-19
      DO 10 I=1,N
      R2(I)=(AN*E(I)+AP*P(I))*(P(I)*E(I)-NI*NI)
10    CONTINUE
      RETURN
      END
C     THIS SUBROUTINE DETERMINES MOBILITIES
      SUBROUTINE MOBLTY(N,MU,DOP,EF,MUP,MUN)
      DIMENSION DOP(N),EF(N),PMU1(900),EMU1(900),F1(900),
     1F2(900),F3(900),G1(900),G2(900),G3(900)
      REAL MU,MUP(N),MUN(N)
      DO 10 I=1,N
      F1(I)=(DOP(I)/((DOP(I)/81.)+2.7E6))
      F2(I)=((EF(I)/7.9E2)**2)/((EF(I)/7.9E2)+.21)
      F3(I)=((EF(I)/3.2E3)**2)
      PMU1(I)=1.+F1(I)+F2(I)+F3(I)
      PMU1(I)=1.+(DOP(I)/((DOP(I)/81)+2.7E5))+(((EF(I)/7.9E2)**2)/((EF
     1(I)/7.9E2)+0.21))+((EF(I)/3.2E3)**2)
      MUP(I)=((PMU1(I))**(-0.5))*480/39
      G1(I)=(DOP(I)/((DOP(I)/350.)+2.E6))
      G2(I)=((EF(I)/4.5E2)**2)/((EF(I)/4.5E2)+1.19)
      G3(I)=((EF(I)/9.6E2)**2)
      EMU1(I)=1.+G1(I)+G2(I)+G3(I)
      EMU1(I)=1.+(DOP(I)/((DOP(I)/350)+2.E5))+(((EF(I)/4.5E2)**2)/((EF
     1(I)/4.5E2)+1.15))+((EF(I)/9.6E2)**2)
      MUN(I)=((EMU1(I))**(-0.5))*1400/39
```

```
10       CONTINUE
         RETURN
         END
C        THIS SUBROUTINE DETERMINES HIGH FIELD GENERATION RATE
         SUBROUTINE  HFG(N,P,E,MUP,MUN,EF,G)
         DIMENSION P(N),E(N),MUP(N),MUN(N),EF(N),G(N),ALPHP(900),ALPHN(90
        10),AEF(900)
         DO 10 I=1,N
         AEF(I)=ABS(EF(I))
         IF(AEF(I).LT.5250)GO TO 20
         ALPHP(I)=7.65E4*EXP(-4.2E5/AEF(I))
         ALPHN(I)=1.3E4*EXP(-2.3E5/AEF(I))
         G(I)=P(I)*MUP(I)*ALPHP(I)*EF(I)+E(I)*MUN(I)*ALPHN(I)*EF(I)
         GO TO 10
20       G(I)=0.0
10       CONTINUE
         RETURN
         END
C        THIS SUBROUTINE DETERMINES COEFFICIENT MATRIX FOR VARIABLE PHIP
         SUBROUTINE COEFF2(N,H2,VA,Z,MUP,SI,R1,R2,G,B,C,D,Q)
         DIMENSION MUP(N),SI(N),R1(N),R2(N),G(N),B(N),C(N),D(N),Q(N)
         INTEGER Z
         DO 10  I=1,N
         IF(I.EQ.1) GO TO 20
         IF(I.EQ.N) GO TO 30
40       B(I)=-MUP(I)*EXP(-(SI(I)+SI(I-1))/2.0)
         D(I)=-MUP(I)*EXP(-(SI(I)+SI(I+1))/2.0)
         C(I)=-B(I)-D(I)
         IF(Z.EQ.2)GO TO 50
         IF(Z.EQ.4) GO TO 50
         Q(I)=H2*(R1(I)+R2(I)-G(I))
         GO TO 10
50       Q(I)=H2*(R1(I)-G(I))
         GO TO 10
20       SI(I-1)=22.263711
         GO TO 40
30       SI(I+1)=9.4980224+VA
         GO TO 40
10       CONTINUE
         Q(1)=Q(1)-B(1)
         Q(N)=Q(N)-D(N)*EXP(VA)
         RETURN
         END
C        THIS SUBROUTINE DETERMINES COEFFICIENT MATRIX FOR VARIABLE PHIN
         SUBROUTINE COEFF3(N,H2,VA,Z,MUN,SI,R1,R2,G,B,C,D,Q)
         DIMENSION MUN(N),SI(N),R1(N),R2(N),G(N),B(N),C(N),D(N),Q(N)
         INTEGER Z
         DO 10 I=1,N
         IF(I.EQ.1) GO TO 20
```

```
         IF(I.EQ.N) GO TO 30
40       B(I)=-MUN(I)*EXP((SI(I)+SI(I-1))/2.)
         D(I)=-MUN(I)*EXP((SI(I)+SI(I+1))/2.)
         C(I)=-B(I)-D(I)
         IF(Z.EQ.2 )GO TO  50
         IF(Z.EQ.4)GO TO 50
         Q(I)=-H2*(R1(I)+R2(I)-G(I))
         GO TO 10
50       Q(I)=H2*(R1(I)-G(I))
         GO TO 10
20       SI(I-1)=22.263711
         GO TO 40
30       SI(I+1)=9.4980224+VA
         GO TO 40
10       CONTINUE
         Q(1)=Q(1)-B(1)
         Q(N)=Q(N)-D(N)*EXP(-VA)
         RETURN
         END
C        THIS SUBROUTINE DETERMINES CURRENT DENSITIES
         SUBROUTINE CRNTS(N,H1,VA,MUP,MUN,PHP,PHN,P,E,JN,JP)
         DIMENSION MUP(N),MUN(N),PHP(N),PHN(N),P(N),E(N),JP(N),JN(N)
         DO 10 I=1,N
         IF(I.EQ.1) GO TO 20
         IF(I.EQ.N) GO TO 30
40       JP(I)=-MUP(I)*P(I)*(PHP(I+1)-PHP(I-1))/(2.*H1)
         JN(I)=-MUN(I)*E(I)*(PHN(I+1)-PHN(I-1))/(2.*H1)
         GO TO 10
20       PHP(I-1)=0.0
         PHN(I-1)=0.0
         GO TO 40
30       PHP(I+1)=VA
         PHN(I+1)=VA
         GO TO 40
10       CONTINUE
         RETURN
         END
C        THIS SUBROUTINE DETERMINES CURRENT GAIN
         SUBROUTINE GAIN(N,JP,JN,R1,R2,X,HFE)
         DIMENSION JP(N),JN(N),R1(N),R2(N),X(N) ,R(900)
         REAL HFE,JC,JB
         JC=JP(N)+JN(N)
         DO 10 I=1,N
         R(I)=R1(I)+R2(I)
10       CONTINUE
         CALL D01GAF(X,R,N,JB,ER,IFAIL)
         IF(IFAIL)40,40,20
20       IF(IFAIL.EQ.1) WRITE(30,*)IFAIL
         IF(IFAIL.EQ.2) WRITE(30,*)IFAIL
```

```
      IF(IFAIL.EQ.3) WRITE(30,*) IFAIL
      STOP
40    HFE=JC/JB
      RETURN
      END
C     THIS SUBROUTINE DETERMINES MAX AND MIN CHANGES IN POTENTIALS
      SUBROUTINE DLM(N,SI,DEL,DELMX,DELMN)
      DIMENSION SI(N),DEL(N)
      DELMN=0.0
      DELMX=0.0
      DO 10 I=1,N
      ADEL=ABS(DEL(I))
      DELMX=AMAX1(DELMX,ADEL)
      DELMN=DELMN+ADEL
10    CONTINUE
      DELMN=DELMN/N
      RETURN
      END
C     THIS SUBROUTINE DETERMINES X BY CROUT'S FACTORISATION METHOD
      SUBROUTINE CROUT(N,B,C,D,Q,X)
      DIMENSION B(N),C(N),D(N),Q(N),X(N),HM(900),PM(900)
      HM(1)=-D(1)/C(1)
      PM(1)=Q(1)/C(1)
      DO 10 I=2,N
      HM(I)=-D(I)/(C(I)+B(I)*HM(I-1))
      PM(I)=(Q(I)-B(I)*PM(I-1))/(C(I)+B(I)*HM(I-1))
10    CONTINUE
      X(N)=PM(N)
      N1=N-1
      DO 20 I=1,N1
      J=N-I
      X(J)=PM(J)+HM(J)*X(J+1)
20    CONTINUE
      RETURN
      END
```

```
      PROGRAM NO.2
C     THIS PROGRAM DETERMINES EMITTER SURFACE CONCENTRATIONS
C     REQUIRED FOR EQUAL EMITTER CHARGE FOR DIFFERENT EMITTER DEPTHS
C     VARIABLE DECLARATION
      REAL VT,LD,NI,H1,XE,NE,NB,NC,BETA,ALPHA,X(100),DOP(100),ENI(100)
     1,Y(100),QE,ER
      INTEGER NN,IFAIL
C     CONSTANTS DECLARATION
      VT=0.026
      LD=34.E-4
      NI=1.5E10
C     NO.OF POINTS CONSIDERED FOR INTEGRATION
      NN=99
C     OUTPUT FILE
      OPEN(UNIT=30,DEVICE='DSK',FILE='QE.1')
C     CONSIDERATION OF DIFFERENT EMITTER DEPTHS
C     K=1  FOR  1MUM EMITTER
C     K=2  FOR  2MUM EMITTER
C     K=3  FOR  4MUM EMITTER
C     K=4  FOR  4.75MUM EMITTER
C     K=5  FOR  8MUM EMITTER
      DO 200 K=2,2
      IF(K.EQ.1)GO TO 10
      IF(K.EQ.2)GO TO 20
      IF(K.EQ.3)GO TO 30
      IF(K.EQ.4)GO TO 40
      IF(K.EQ.5)GO TO 50
10    XE=(1.E-4)/LD;GO TO 70
20    XE=(2.E-4)/LD;GO TO 70
30    XE=(4.E-4)/LD;GO TO 70
40    XE=(4.75E-4)/LD;GO TO 70
50    XE=(8.E-4)/LD;GO TO 70
C     DOPING PROFILE PARAMETERS
70    NE=(7.E19)/NI
      NB=(2.E17)/NI
      NC=(2.E14)/NI
      BETA=1.2
      ALPHA=ALOG(NE/(NB*EXP(-BETA)-NC))
C     STEP DISTRIBUTION
      H1=XE/NN
      X(1)=0.0
      DO 100 I=1,NN
      J=I+1
      X(J)=I*H1
100   CONTINUE
```

```
      N=NN+1
C     DETERMINATION OF DOPING PROFILE
      DO 350 I=1,N
      DOP(I)=NE*EXP(-ALPHA*((X(I)/XE)**2))-NB*EXP(-BETA*((X(I)/XE)**2)
     1)+NC
350   CONTINUE
      CALL NIEFF(N,VT,NI,DOP,ENI)
      DO 320 I=1,N
      Y(I)=DOP(I)/ENI(I)
320   CONTINUE
      IFAIL=1
      CALL D01GAF(X,Y,N,QE,ER,IFAIL)
      IF(IFAIL)440,440,330
330   WRITE(30,*)IFAIL
440   XE=XE*LD;NE=NE*NI;WRITE(30,*) XE,NE,QE,ER
200   CONTINUE
      STOP
      END
C     THIS SUBROUTINE DETERMINES BGN CORRECTION TO NI
      SUBROUTINE NIEFF(N,VT,NI,DOP,ENI)
      DIMENSION DOP(N),ENI(N),F(100),ADOP(100)
      REAL NI
      DO 10 I=1,N
      XL=(1.E17)/NI
      ADOP(I)=ABS(DOP(I))
      IF(ADOP(I).GE.XL) GO TO 20
30    ENI(I)=1.
      GO TO 10
20    F(I)=ALOG(ADOP(I)/XL)
      ENI(I)=EXP((9.E-3)*(F(I)+SQRT(F(I)*F(I)+0.5))/VT)
10    CONTINUE
      RETURN
      END
```